Comparison of Damped Oscillations in Solar and Stellar X-ray flares

I.-H. Cho[1,2], K.-S. Cho[1,2,+], V. M. Nakariakov[3,4,5], S. Kim[1], P. Kumar[1]

ABSTRACT

We explore the similarity and difference of the quasi-periodic pulsations (QPPs) observed in the decay phase of solar and stellar flares at X-rays. We identified 42 solar flares with pronounced QPPs, observed with the Reuven Ramaty High-Energy Solar Spectroscopic Imager (RHESSI) and 36 stellar flares with QPPs, observed with X-ray Multi Mirror Newton observatory (XMM-Newton). The Empirical Mode Decomposition (EMD) method and least-square fit by a damped sine function were applied to obtain the periods (P) and damping times (τ) of the QPPs. We found that (1) the periods and damping times of the stellar QPPs are 16.21±15.86 min and 27.21±28.73 min, while those of the solar QPPs are 0.90±0.56 and 1.53±1.10 min, respectively. (2) The ratio of the damping times to the periods (τ/P) observed in the stellar QPPs (1.69±0.56) are statistically identical to those of solar QPPs (1.74±0.77). (3) The scalings of the QPP damping time with the period are well described by the power law in both solar and stellar cases. The power indices of the solar and stellar QPPs are 0.96±0.10 and 0.98±0.05, respectively. This scaling is consistent with the scalings found for standing slow magnetoacoustic and kink modes in solar coronal loops. Thus, we propose that the underlying mechanism responsible for the stellar QPPs is the natural magnetohydrodynamic oscillations in the flaring or adjacent coronal loops, as in the case of solar flares.

Subject headings: Sun: flares – Sun: oscillations – Stars: low-mass – Star: flares – Star: oscillations – Methods: observational

---

[1]Korea Astronomy and Space Science Institute, Daejeon 305-348, Korea

[2]University of Science and Technology, Daejeon 305-348, Korea

[3]School of Space Research, Kyung Hee University, Yongin, 446-701, Korea

[4]Centre for Fusion, Space & Astrophysics, Physics Department, University of Warwick, Coventry CV4 7AL, UK

[5]Astronomical Observatory at Pulkovo, Russian Academy of Sciences, 196140 St. Petersburg, Russia

[+]Corresponding author (kscho@kasi.re.kr)

1. INTRODUCTION

X-ray light curves of solar flares contain quasi-periodic pulsations (QPPs, e.g., Nakariakov 2007; Nakariakov & Melnikov 2009), which are detected before and during the impulsive phase (e.g., Antonucci et al. 1984; Fárník et al. 2003; Inglis et al. 2008), and in the decay phase (e.g., Kim et al. 2012; Kumar et al. 2013, 2015) of the flares. QPPs are found to be a common feature of solar flaring lightcurves associated with both thermal (Simões et al. 2015) and non-thermal emission (Kupriyanova et al. 2010). In the impulsive phase, QPPs might be explained by a repetitive regime of spontaneous magnetic reconnection ("magnetic dripping", see Nakariakov et al. 2010), such as periodic shedding of plasmoids (e.g., Kliem et al. 2000; Bárta et al. 2008; Kumar & Cho 2013); or by an effect of magnetohydrodynamic (MHD) oscillations: variation of the plasma and magnetic field parameters, which changes the efficiency of the gyrosynchrotron emission (e.g., Stepanov et al. 2004; Khodachenko et al. 2006; Kuznetsov et al. 2015); periodically change the non-thermal particle kinematics (e.g., Zaitsev & Stepanov 1982), or periodically trigger magnetic reconnection by MHD oscillations (Chen & Priest 2006; Nakariakov et al. 2006). The modulating MHD oscillations could be confined to the flaring site, or could occur in plasma structures situated nearby. In particular, one possibility is the leakage of sunspot oscillations in the corona in a form of slow magnetoacoustic waves (e.g., DeMoortel 2009; Reznikova & Shibasaki 2011; Sych & Nakariakov 2014; Cho et al. 2015) which reach the coronal reconnection sites and periodically trigger or modulate the process of reconnection (e.g., Chen & Priest 2006; Sych et al. 2009; Kumar et al. 2016). In the decay phase of flares, QPPs could be explained in terms of natural oscillations the flaring loops, e.g. standing kink or slow-mode waves. These waves can be directly or indirectly excited by an impulsive source associated with the flare or CME (e.g., Aschwanden et al. 2002; Nakariakov et al. 2004; Tsiklauri et al. 2004; Selwa et al. 2005; Selwa & Ofman 2010; Zimovets & Nakariakov 2015). QPPs have been detected at many wavelengths, from radio (e.g., Wright & Nelson 1987; Qin et al. 1996; Grechnev et al. 2003; Nakariakov et al. 2003) to extreme ultraviolet (EUV) (e.g., Wang et al. 2003), X-ray (e.g., Harrison 1987; Li & Gan 2008; Ning 2014), and gamma-ray (Nakariakov et al. 2010).

An important class of oscillations observed in the decay phase of solar flares are so-called SUMER oscillations, first detected as periodic Doppler shifts with the Solar Ultraviolet Measurements of Emitted Radiation (SUMER, Wilhelm et al. 1995) in hot (>6 MK) coronal loops (e.g., Wang et al. 2002; Wang 2011). Wang et al. (2003) performed a statistical study on the 54 QPPs observed in the Doppler-shift and soft X-ray intensity of the hot coronal loops, and established that the oscillations have periods of 7–31 min with decay times 5.7–36.8 min. Mariska (2006) detected similar Doppler-shift oscillations with periods of 5.5 min observed by the Bragg Crystal Spectrometer (BCS, Lang et al. 1992) which probed hotter plasma ($\sim$ 12–14 MK) comparing to SUMER. Recently, the high-resolution observation with

the Atmospheric Imaging Assembly (AIA Lemen et al. 2012) onboard the Solar Dynamics Observatory (*SDO*, Pesnell et al. 2012), evidenced that oscillations in the hot coronal loops are excited by an energy release at one of the footpoints of the arcade loops (Kumar et al. 2013, 2015). These observational findings are consistent with the interpretation of SUMER oscillations in terms of slow magnetoacoustic waves (Ofman & Wang 2002; Nakariakov et al. 2004; Taroyan et al. 2005).

QPP are also frequently detected in stellar flares, e.g., in wide-band optical wavelengths (e.g., Rodono 1974; Mullan et al. 1992; Houdebine et al. 1993; Mathioudakis et al. 2003, 2006; Anfinogentov et al. 2013), which are difficult to be detected in the Sun. A systematic study of QPPs in stellar white light flares was recently performed by Balona et al. (2015); Pugh et al. (2016). Typically, stellar QPP are seen as a periodic, decaying variation of the signal after the flare peak, which resembles SUMER oscillations in solar flares. Unfortunately, there is no observational example of QPPs in a solar white light flare, so that the direct comparison is difficult. However, Pugh et al. (2015) recently observed a multi-periodic oscillation in a stellar white light flare, that supports the interpretation of stellar QPP as natural MHD oscillations of the flaring loops.

Various aspects of stellar flares, including powerful super-flares seemed to be similar to those of solar flares (e.g., Aschwanden et al. 2008; Maehara et al. 2012). The similarity in solar and stellar flares, including the QPPs may give us hints to understand the nature of the flares and associated oscillations, as well as coronal plasma properties for various stars including the Sun (Balona et al. 2015; Chang et al. 2015). In particular, properties of oscillating loops could be estimated by applying an appropriate model to the frequency and amplitude modulation of the perturbation, which are independent on the sharpness and strength of the sources. Particularly, stellar X-ray flares can provide proper parameters such as the emission measure, temperature, abundance, and density of the flaring loops (e.g., Raassen et al. 2007; Pandey & Karmakar 2015), which are essential for the indirect determination of the coronal magnetic field strength. First attempts to use QPP for stellar coronal seismology have been made by Mitra-Kraev et al. (2005); Pandey & Srivastava (2009); Anfinogentov et al. (2013); Srivastava et al. (2013).

In this work, we perform a comparative study of QPPs in the decay phase of solar and stellar flares, aiming to establish relationships of these phenomena, and reveal whether they have similar or different characteristics. To minimise a possible selection effect from different wavelengths, we consider data obtained in the energy bands 3–12 keV of the Reuven Ramaty High-Energy Solar Spectroscopic Imager (RHESSI, Lin et al. 2002) for solar flares, and 0.3–2 keV of the X-ray Multi Mirror Newton observatory (XMM-Newton, Jansen et al. 2001). In this study we consider cool dwarf stars, because the envelope layers of those stars

are convective and thus their coronal magnetic activities could be assumed to be similar to the Sun.

In Section 2, we describe the data-sets analysed, and present the method used to detect the oscillatory patterns in the signals. In Section 3, we show the relationships between the periods and damping times observed in both solar and stellar flares. Finally, we summarise and discuss our results.

2. DATA and METHODS

2.1. QPPs in Solar Flares

We have selected 59 events with clear QPPs in the solar X-ray flares occurred in 2014, and observed with RHESSI. This instrument was designed to investigate particle acceleration and impulsive energy releases in solar flares, delivering the imaging and spectroscopic information in X-ray/gamma-ray bands. It covers the energy range from soft X-rays, from 3 keV, up to gamma-rays, 17 MeV. Figure 1 shows an example of a solar flare occurred on 30 Oct 2014 at 01:33:10 UT, observed also by the SDO/AIA. **The CLEAN algorithm is used to reconstruct the RHESSI image with 1 min integration time (Hurford et al. 2002, and references therein).** The flare locations were given by the RHESSI flare list[1]. Light curves were obtained by integrating the X-ray signal over the whole flaring site at 3–25 keV. First, the flare was identified in the low energy channel, 3–6 keV, where the signal is typically the strongest, by eye. Then, if the correlation coefficient between the lowest energy signal and the signals obtained at 6–12 keV and 12–25 keV bands was higher than 0.95, those signals were also taken in consideration. The list of the flares used in this study is presented in Table 1. The first three columns represent the epochs of the flares. The 4th and 5th columns are the positions where the flares occurred.

Figure 2 shows how we detected the QPP patterns in the X-ray light curves. The top panel shows the time variation of the X-ray count rate of the flare shown in Figure 1. To detect a QPP effectively, the smooth trend should be properly removed from the signal, as it may affect the spectral behaviour of the residual power spectrum (e.g. Chang 2014; Mariska 2006). We obtained the trend by applying the Empirical Mode Decomposition (EMD, Huang et al. 1998). The EMD efficiently decomposes the original time series into the Intrinsic Mode Functions (IMFs). In particular, the IMF with the slowest characteristic time scale may be used as a trend of the original signal. The advantage of this approach is its independence of

[1]http://hesperia.gsfc.nasa.gov/hessidata/dbase/hessi_flare_list.txt

any assumptions that are intrinsic in other de-trending methods, for example the spectral band and filter function of low-frequency filtering, the time duration of smoothing, the form and parameters of best-fitting detrending function, etc. This highly adaptive method has been specifically designed for the analysis of non-linear and non-stationary time series, and has been successfully applied to the analysis of various solar and geophysical phenomena (e.g., Wu et al. 2011; Kolotkov et al. 2015a,b).

In this study, the trends are defined as a sum of several lowest frequency IMFs allowing us to remove the steep decreasing pattern typical for flares. The residual is the sum of the remaining IMFs. If the residual includes the IMF which shows a damped oscillatory pattern, it was fitted with a damped harmonic function, $I = A\exp[-(t-t_0)/\tau]\sin[(t-t_0)/P - B]$, where A, t_0 and B are the amplitude, starting time, and phase of the oscillation, respectively. We set the starting time of the sine function equal to the starting time of the exponential function, which was after the flare peak time by adjusting the initial values. In panel (b), the residual (black) and the best-fitting QPP (blue) are presented. The best-fitting curve is shown by the dashed line in the panel (c). The panel (d) shows the power spectrum of the residual. Because the EMD always produces the quasi-periodic signals for the IMFs, the obtained period of the damped sine function should be tested by calculating the residual power spectrum. The vertical line in this panel is the period obtained from the damped sine fitting. The red, yellow, and green lines are the 99%, 95%, and 90% confidence intervals. The significance are defined by the Fisher randomisation method (Linnell Nemec & Nemec 1985; Yuan et al. 2011; Yu et al. 2013). The confidence interval for each frequency is determined from the cumulative probability of the 10,000 noise powers at each frequency. The peak periods in the power spectra are slightly different from periods of the best-fitting curve. It may be attributed to the non-linear nature of the QPPs. However, we check whether the fitted periods are within the half width of the significant peaks in the power spectrum, and found that in the majority of the analysed lightcurves, most of the best-fitting periods satisfied this condition. The periods and damping times with the significance levels estimated in the solar QPPs are presented in Table 1.

Figure 3 shows the fitting results for QPPs in all 59 solar flares. The number in each panel denotes the flare ID in Table 1. The horizontal and vertical scales are normalized by the damping time and amplitude of the exponentially decaying harmonic functions, respectively, as it is shown in the enlarged version of the flare # 1. The scales of the horizontal and vertical axes in all small panels are omitted for the visualisation purposes. Each panel is similar to the plot shown in Figure 2(c).

2.2. QPPs in Stellar Flares

We also selected 52 QPPs in lightcurves of stellar X-ray flares detected in the 0.3–2 keV band of the XMM-Newton. The telescope includes the European Photon Imaging Camera (EPIC, Struder et al. 2001; Turner et al. 2001), the Reflection Grating Spectrometer (RGS denHerder et al. 2001), and the Optical Monitor (OM, Mason et al. 2001). The EPIC consists of pn-CCD (0.15–15 keV) and two MOS-CCD (0.1–10 keV) which almost continuously registers photons as events. The mean time cadence of light curves is about 60 s, ranging from 10 to 300 s. The cadence time was not same for different flares. The original time cadence of XMM-Newton data is less than one second, but to improve the signal-to-noise ratio we binned the data. To determine the appropriate binning time, we first applied the 60 s binning. If the data still looked too noisy, we then applied a longer-time binning, e.g. 120 s, etc., until the binned data are not too noisy. This approach led to different binning times for different events.

Our targets include 16 dwarf stars (CN Leo, HD179949, YZ Canis Minoris, 47 Cas, GJ674, HD189733, AU Mic, 61 Cyg, LP412-31, Proxima Cen, ξ Boo, YY Gem, Ross 154, At Mic, κ^1 Cet and SCR J1845-6357), two binary dwarfs with a white dwarf as a companion (V471 Tauri and AE Aqr), 4 serendipitous flares in the open clusters (Zeta Orion, BL Hyi, IC2602, and Blanco 1). All of these targets are known either as flare producing stars or having flare-producing companions (Choi et al. 1999; Robinson et al. 1999; Tsikoudi & Kellett 2000; Güdel et al. 2001; Magee et al. 2003; Güdel et al. 2004; Trenholme et al. 2004; Shkolnik et al. 2005; Stelzer et al. 2006; Stepanov et al. 2006; Watson et al. 2006; Pandey & Singh 2008; Robrade et al. 2010; Liefke et al. 2010; Pillitteri et al. 2010; Fuhrmeister et al. 2011; Robrade et al. 2012; Scandariato et al. 2013; Bhatt et al. 2014; Pillitteri et al. 2014; Bhatt et al. 2014; Pandey & Karmakar 2015). The list of targets, including XMM-Newton ObsID with its source and background regions used for the light curve extractions are given in Table 2.

The light curves are extracted by using the XMM-Newton Science Analysis System (SAS[2]) version 14.0. We only use the 0.3–2 keV energy band to avoid emission associated with non-thermal particles (e.g., Pandey & Karmakar 2015). For pre-processing, the SAS task `em(p)roc` was used. The source and background light curves were obtained by using the SAS `evselect`. The light curve corrections are performed by using the SAS `epiclccorr`. The source regions were selected as annuli to avoid the pile-up effect due to photons from a bright source. The inner radius of the annulus is determined after checking the energy spectrum by using the SAS `epatplot`. If the datasets are free from the pile-up effect, we use the circle for the source region. The background region is selected in the same CCD where

[2]http://heasarc.gsfc.nasa.gov/docs/xmm/abc/

the source region was defined.

The analysis of QPPs in the stellar flare lightcurves was performed similarly to the solar flare analysis (Sec. 2.1). Figure 4 shows the analysis of a typical stellar flare that occurred at the M8 dwarf LP412-31. The panel (a) is the X-ray lightcurve with the trend. The panel (b) gives the residual and the damped oscillatory IMF. The panel (c) shows the comparison of the damped oscillatory IMF with the best-fitting damped harmonic curve. The bottom panel (d) shows the power spectrum of the residual. QPP patterns detected in 52 stellar flares are demonstrated in Figure 5. The number in each panel corresponds to the Flare ID in Table 2. The determined periods, damping times and significance levels are also presented in Table 2.

3. RESULTS

Figure 6 shows the histograms of the periods (top), damping times (middle), and their ratios that can be considered as the quality-factors (bottom), found in the analysed solar and stellar QPPs. The cases with the detection of a periodicity above the confidence level higher than 80% were considered as significant. The insignificant samples were excluded from the further analysis. The vertical dashed lines in each panel indicates mean values of the periods, damping times, and their ratios obtained for the 42 solar and 36 stellar flares in which the detected QPP were significant. Thus, the significant detected periods in the solar and stellar QPPs are 0.90±0.56 and 16.21±15.86 min, respectively. The damping times are 1.53±1.10 and 27.21±28.73 min, respectively. The overall shapes of the distributions observed in the solar and stellar QPPs are similar to each other. The characteristic scales of the periods and damping times detected in the stellar QPPs are much longer than the solar QPPs. The quantitative difference may come from the different lengths and temperatures of the stellar coronal loops. On the other hand, the ratio of the damping times τ to the periods P of the solar and stellar QPPs are τ/P =1.74±0.77 and 1.69±0.56, respectively, which seem to be identical. To check whether they are the same or not, we performed the statistical Kolmogorov–Smirnov (K-S) test. The p-value of the K-S test is 0.93 which cannot reject the null-hypothesis that the two distributions of the τ/P observed in the solar and stellar QPPs are the same. The statistics of the periods and damping times are presented in Table 3.

Figure 7 shows the scaling of the damping times and periods observed in both the solar (left) and stellar (right) QPPs. The best-fitting straight lines in the left and right panels are the power-law dependency ($\tau = 1.59 \pm 1.07 P^{0.96\pm0.10}$ and $\tau = 1.70 \pm 1.13 P^{0.98\pm0.05}$), respectively. Both power law indices are comparable with those observed in the transverse and longitudinal oscillations of the solar flaring or coronal loops in the previous studies (c.f.

Ofman & Wang 2002; Wang et al. 2003; Goddard et al. 2016). In Figure 8, we plot the damping times as a function of the periods for both solar and stellar QPPs. The black straight line is $\tau = 1.62 \pm 1.05 P^{0.99 \pm 0.03}$ which is obtained from the joint, solar and stellar scaling.

4. Conclusion and Discussion

Analysis of soft X-ray lightcurves of solar and stellar flares by applying the Empirical Mode Decomposition method, revealed the presence of 42 QPPs in solar flares and and 36 QPPs in stellar flares. We performed the least-square-fitting of the detected oscillatory patterns, with the damped harmonic function to the QPPs, allowing us to estimate the periods (P) and damping times (τ) of the QPPs. Most of the periods determined by fitting are well matched with the peak periods in the power spectra of the detrended lightcurves. We found that the periods and damping times of stellar QPPs are 16.21±15.86 min and 27.21±28.73 min, respectively. These values are longer than those of obtained in solar QPPs 0.90±0.56 min and 1.53±1.10 min. The ratios (τ/P) of the solar (1.74±0.77) and stellar (1.69±0.56) QPPs are found to be statistically identical.

We found that the scalings of the damping time τ with the oscillation period are well fitted with a power-law dependency in the form $\tau = aP^b$ in both the solar and stellar QPPs. The amplitudes a for solar and stellar flares are found to be 1.59±1.07 and 1.70±1.13, respectively. The power indices b for solar and stellar flares are 0.96±0.10 and 0.98±0.05, respectively. These values are very close to each other, and also comparable with the values observed in the solar coronal loop oscillations. For example, Wang et al. (2003) reported that the power index was 1.06 ± 0.18 in a set of 49 slow magnetoacoustic standing (SUMER) oscillations in coronal loops. Ofman & Wang (2002) found the power index to be 1.17±0.34 in a set of 11 transverse loop oscillations. Thus, the main result of this study is the apparent similarity of the scaling laws of the damping times and periods of QPPs in solar and stellar flares. This finding indicates that the underlying mechanism responsible for stellar QPPs detected in the soft X-ray emission after the flare peaks is likely to be of the same nature as in solar flares, and could be the natural magnetoacoustic oscillations of the flaring or adjacent coronal loops. A similar conclusion has recently been drawn by Pugh et al. (2015), based on the detection of multiple periodicities in a stellar flare. However that result was obtained in the white light band, which makes difficult the direct comparison with solar flares. In contrast, our results are obtained in the soft X-ray band that is a commonly-used band for the detection of solar flares, allowing for the direct comparison of solar and stellar results.

The periods obtained in the solar QPPs in our study are much shorter than the periods

of the slow-mode standing wave obtained by Wang et al. (2003), 7–31 min. The discrepancy may come from the selection effect of the instruments as explained by Wang (2011). The RHESSI energy band (3–25 keV) used in this study is associated with hotter loops (Ryan et al. 2014; Caspi et al. 2014) comparing to the SUMER oscillation loops, that can result in the higher sound speeds. Moreover, typically the flaring loops are much shorter than the long loops hosting SUMER oscillations, and it also contributes to the decrease in the periods of slow modes detected in soft X-rays. In addition, in flaring loops the slow oscillations may be on the second longitudinal harmonic, if they are excited simultaneously at both foot points, e.g. by the precipitating non-thermal electrons going down from the reconnection cite along the legs of the loop (e.g. Nakariakov et al. 2004). The second harmonics have the oscillation period about two times shorter than of the fundamental mode. Thus, it is natural to expect that soft X-ray QPPs are of shorter periods than EUV QPPs. We would also point out that our results are consistent with the 9.6–61.6 s intensity oscillations in the coronal loops observed by Soft X-ray Telescope (SXT) on Yohkoh, reported by McKenzie & Mullan (1997).

In general, QPPs in flares could be produced by several different mechanisms. These mechanisms could be roughly divided in three groups: the modulation of the emitting plasma or the kinematics of non-thermal electrons by an MHD oscillation and a quasi-periodic regime of magnetic reconnection, induced by an MHD oscillation, and a spontaneous quasi-periodic magnetic reconnection - "magnetic dripping" (see Nakariakov et al. 2016, for a recent review). The apparent similarity of the time profiles of the QPPs detected in this study, the rapidly exponentially decaying trains of oscillations, with the properties of MHD oscillations observed with high spatial resolution in solar coronal plasma structures indicates that the observed QPPs are likely to be associated with MHD oscillations.

The recent study of Inglis et al. (2015) showed the importance of accounting for the effect of coloured noise in the determination of the statistical significance of the spectral peaks associated with QPP. However Simões et al. (2015) demonstrated that QPPs are present in 80% of X-class solar flares in Cycle 24. In our study we concentrate on the QPP signals that have a specific shape, namely the rapidly decaying harmonic oscillations. The search for a signal of this specific shape is motivated by the unequivocal detection of such signals in solar coronal observations with high spatial resolution (e.g., Kumar et al. 2015; Zimovets & Nakariakov 2015). This approach reduces significantly the false detection probability, as in this work we also account for the phase information, making our findings more robust.

Observations of stellar flares are intrinsically unimaged, hence it is impossible to estimate directly one of the key parameters of a coronal MHD oscillation, its wavelength, by the length of the oscillating loop. However, the use of certain scalings could provide some useful, order of magnitude estimations (e.g., Mullan et al. 2006), linking the flaring loop length with the emission measure and the decay time of the flare. It should be done on the ad hoc basis, as the same star may have flares in active regions of quite different geometrical sizes, as one can see in solar flares. Likewise, the estimations of flaring loop lengths in Mullan et al. (2006) show a rather broad range too, for example for the analysed flares on AD Leo, the lengths range from 37 to 340 Mm. Nevertheless, the use of such technique in combination with the seismological technique is an interesting topic for a follow up study. We speculate that the flaring emission comes from a small region in the vicinity of the flare site, as it is observed in solar flares. More specifically, the soft X-ray emission studied here, comes from a flaring loop or arcade. As the detected periods of stellar QPP are systematically longer than of solar QPP, and as the temperature of the emitting plasma is not likely to differ by more than a factor of 5, making the sound speed about two times higher maximum than in the solar flares, we may conclude that the lengths of the stellar flare loops are typically longer than in solar flares.

Several previous seismological studies for stellar QPPs gave insight into identifying the MHD mode responsible for the QPP. For example, Mitra-Kraev et al. (2005) interpreted the soft X-ray QPP in a flare the dwarf AT Mic, as a standing slow magnetoacoustic oscillation. This interpretation allowed the authors to estimate the temperature of the flaring loop as 13 MK. Srivastava et al. (2013) observed multiple QPPs in a flare on the Proxima Cen. The measured temperature of the oscillating region was 7.2 MK. The authors interpreted the QPP as a standing slow magnetoacoustic wave in the flaring loop. Pandey & Srivastava (2009) observed a QPP in a flare on the dwarf ξ Boo, and interpreted it as a kink oscillation. The loop length was estimated as 380 Mm with the mean magnetic field of 36 G. (Un)fortunately, our study does not allow us to discriminate between the longitudinal and transverse oscillations, as in the solar case the power indices of the scaling of the decay time with oscillation periods are almost identical. Therefore, we leave this issue for a follow-up study.

The variety of the time scales in the periods and damping times observed in the stars may reflect the variety of the properties of the stellar coronae such as the temperatures or lengths of the oscillating loops. More quantitative estimation can be made with the use of spectral observations, which is beyond the scope of our study.

This work is supported by the "Planetary system research for space exploration" from Korea Astronomy and Space Science Institute. VMN is supported by the European Research Council under the project No. 321141 SeismoSun and the BK21 plus program of the National Research Foundation funded by the Ministry of Education of Korea. We appreciate anonymous referee which improves the manuscript.

REFERENCES

Anfinogentov, S., Nakariakov, V. M., Mathioudakis, M., et al. 2013, ApJ, 773, 156

Antonucci, E., Gabriel, A. H., & Patchett, B. E. 1984 Sol. Phys., 93, 85

Aschwanden, M. J., de Pontieu, B., Schrijver, C. J., & Title, A. M. 2002, Sol. Phys., 206, 99

Aschwanden, M. J., Stern, R. A., Güdel, M. 2008, ApJ, 672, 659-673

Balona, L. A., Broomhall, A.-M., Kosovichev, A., et al. 2015, MNRAS, 450, 956

Bárta, M., Karlický, M., & Žemlička. R 2008, Sol. Phys., 253, 173

Bhatt, H., Pandey, J. C., Singh, K. P., et al. 2014, J. Astroph. Astron., 35, 39

Caspi, A., Krucker, S., & Lin, R. P. 2014, ApJ, 781, 43

Chang, H.-Y. 2014, Publ. Astron. Soc. Jpn., 66, 86

Chang, S.-W., Byun, Y.-I., & Hartman, J. D. 2015, ApJ, 814, 35

Chen, P. F., & Priest, E. R. 2006, Sol. Phys., 238, 313

Choi, C.-S., Dotani, T., & Agrawal, P. C. 1999, ApJ, 525, 399

Cho, K.-S., Bong, S.-C., Nakariakov, V. M., et al. 2015, ApJ, 802, 45

De Moortel, I. 2009, Space Sci. Rev., 149, 65

den Herder, J. W., Brinkman, A. C., Kahn, S. M., et al. 2001, A&A, 365L, 7

Fárník, F., Karlický, M., & Švestka, Z. 2003, Sol. Phys., 218, 183

Fuhrmeister, B., Lalitha, S., Poppenhaeger, K., et al. 2011, A&A, 534, 133

Goddard, C. R., Nisticò, G., Nakariakov, V. M., & Zimovets, I. V. 2016, A&A, 585, A137

Grechnev, V. V., White, S. M., & Kundu, M. R. 2003, ApJ, 588, 1163

Güdel, M., Audard, M., Magee, H., et al. 2001, A&A, 365, 344

Güdel, M., Audard, M., Reale, F., et al. 2004, A&A, 416, 713

Harrison, R. A. 1987, A&A, 182, 337

Houdebine, E. R., Foing, B. H., Doyle, J. G., & Rodono, M. 1993, A&A, 274, 245

Huang, N. E., Shen, Z., Long, S. R., et al. 1998, Proceedings of the Royal Society of London Series A, 454, 903

Hurford, G. J., Schmahl, E. J., Schwartz, R. A., et al. 2002, Sol. Phys., 210, 61

Inglis, A. R., Nakariakov, V. M., & Melnikov, V. F. 2008, A&A, 487, 1147

Inglis, A. R., Ireland, J., & Dominique, M. 2015, ApJ, 798, 108

Jansen, F., Lumb, D., Altieri, B., et al. 2001, A&A, 365L, 1

Khodachenko, M. L., Rucker, H. O., Kislyakov, A. G., Zaitsev, V. V., & Urpo, S. 2006, Space Sci. Rev., 122, 137

Kim, S., Nakariakov, V. M., & Shibasaki, K. 2012, ApJ, 756L, 36

Kliem, B., Karlický, M., & Benz, A. O. 2000, A&A, 360, 715

Kolotkov, D. Y., Broomhall, A.-M., & Nakariakov, V. M. 2015, /mnras, 451, 4360

Kolotkov, D. Y., Nakariakov, V. M., Kupriyanova, E. G., et al. 2015, A&A, 574, 53

Kumar, P., & Cho, K.-S. 2013, A&A, 557, A115

Kumar, P., Innes, D. E., & Inhester, B. 2013, ApJ, 779L, 7

Kumar, P., Nakariakov, V. M., & Cho, K.-S. 2015, ApJ, 804, 4

Kumar, P., Nakariakov, V. M., & Cho, K.-S. 2016, ApJ, 822, 7

Kupriyanova, E. G., Melnikov, V. F., Nakariakov, V. M., & Shibasaki, K. 2010, Sol. Phys., 267, 329

Kuznetsov, A. A., Van Doorsselaere, T., & Reznikova, V. E. 2015, Sol. Phys., 290, 1173

Lang, J., Bentley, R. D., Brown, C. M. 1992, Publ. Astron. Sco. Japan, 44, 55

Lemen, J, R., Title, A, M., Akin, D, J., et al. 2012, Sol. Phys., 275, 17

Liefke, C., Fuhrmeister, B., & Schmitt, J. H. M. M. 2010, A&A, 514, 94

Li, Y. P., & Gan, W. Q. 2008, Sol. Phys., 247, 77

Lin, R. P., Dennis, B. R., Hurford, G. J., et al. 2002, Sol. Phys., 210, 3

Linnell Nemec, A. F., & Nemec, J. M. 1985, AJ, 90, 2317

Maehara, H., Shibayama, T., Notsu, S., et al. 2012, Nature, 485, 478

Magee, H. R. M., Güdel, M., Audard, M., & Mewe, R. 2003, Adv. Space Res., 32, 1149

Mariska, J. T. 2006, ApJ, 639, 484

Mason, K. O., Breeveld, A., Much, R., et al. 2001, A&A, 365L, 36

Mathioudakis, M., Seiradakis, J. H., Williams, D. R., et al. 2003, A&A, 403, 1101

Mathioudakis, M., Bloomfield, D. S., Jess, D. B., Dhillon, V. S., & Marsh, T. R. 2006, A&A, 456, 323

McKenzie, D. E., & Mullan, D. J. 1997, Sol. Phys., 176, 127

Mitra-Kraev, U., Harra, L. K., Williams, D. R., & Kraev, E. 2005, A&A, 436, 1041

Mullan, D. J., Herr, R. B., & Bhattacharyya, S. 1992, ApJ, 391, 265

Mullan, D. J., Mathioudakis, M., Bloomfield, D. S., & Christian, D. J. 2006, ApJS, 164, 173

Nakariakov, V. M., Melnikov, V. F., & Reznikova, V. E. 2003, A&A, 412L, 7

Nakariakov, V. M., Tsiklauri, D., Kelly, A., et al. 2004, A&A, 414L, 25

Nakariakov, V. M., Foullon, C., Verwichte, E., & Young, N. P. 2006, A&A, 452, 343

Nakariakov, V. M. 2007, Adv. Space Res., 39, 1804

Nakariakov, V. M., & Melnikov, V. F. 2009, Space Sci. Rev., 149, 119

Nakariakov, V. M., Foullon, C., Myagkova, I. N., & Inglis, A. R. 2010, ApJ, 708L, 47

Nakariakov, V. M., Inglis, A. R., Zimovets, I. V., et al. 2010, Plasma Physics and Controlled Fusion, 52, 124009

Nakariakov, V. M., Pilipenko, V., Heilig, B., et al. 2016, Space Sci. Rev., 200, 75

Ning, Z. 2014, Sol. Phys., 289, 1239

O'Shea, E., Banerjee, D., Doyle, J. G., et al. 2001, A&A, 368, 1095

Ofman, L., & Wang, T. 2002, ApJ, 580, L85

Pandey, J. C., & Singh, K. P. 2008, MNRAS, 387, 1627

Pandey, J. C., & Srivastava, A. K. 2009, ApJ, 697L, 153

Pandey, J. C., & Karmakar, S. 2015, ApJ, 149, 47

Pesnell, W. D., Thompson, B. J., & Chamberlin, P. C. 2012, Sol. Phys., 275, 3

Pillitteri, I., Wolk, S. J., Cohen, O., et al. 2010, ApJ, 722, 1216

Pillitteri, I., Wolk, S. J., Lopez-Santiago, J., et al. 2014, ApJ, 785, 145

Pugh, C. E., Nakariakov, V. M., & Broomhall, A.-M. 2015, ApJ, 813, 5

Pugh, C. E., Armstrong, D. J., Nakariakov, V. M., & Broomhall, A.-M. 2016, MNRAS, 459, 3659

Qin, Z., Li, C., Fu, Q., & Gao, Z. 1996, Sol. Phys., 163, 383

Raassen, A. J. J., Mitra-Kraev, U., & Güdel, M. 2007, MNRAS, 379, 1075

Reznikova, V. E., & Shibasaki, K. 2011, A&A, 525A, 112

Robinson, R. D., Carpenter, K. G., & Percival, J. W. 1999, ApJ, 516, 916

Robrade, J., Poppenhaeger, K., & Schmitt, J. H. M. M. 2010, A&A, 513, 12

Robrade, J., Schmitt, J. H. M. M., & Favata, F. 2012, A&A, 543, 84

Rodono, M. 1974, A&A, 32, 337

Ryan, D. F., O'Flannagain, A. M., Aschwanden, M. J., & Gallagher, P. T. 2014, Sol. Phys., 289, 2547

Scandariato, G., Maggio, A., Lanza, A. F., et al. 2013, A&A, 552, 7

Selwa, M., Murawski, K., & Solanki, S. K. 2005, A&A, 436, 701

Selwa, M., & Ofman, L. 2010, ApJ, 714, 170

Simões, P. J. A., Hudson, H. S., & Fletcher, L. 2015, Sol. Phys., 290, 3625

Shkolnik, E., Walker, G. A. H., Bohlender, D. A., et al. 2005, ApJ, 622, 1075

Srivastava, A. K., Lalitha, S., & Pandey, J. C. 2013, ApJ, 778L, 28

Stelzer, B., Schmitt, J. H. M. M., Micela, G., & Liefke, C. 2006, A&A, 460, 35

Stepanov, A. V., Kopylova, Y. G., Tsap, Y. T., et al. 2004, Astronomy Letters, 30, 480

Stepanov, A. V., Tsap, Yu. T., & Kopylova, Yu. G. 2006, Astronomy Letters, 32, 569

Strüder, L., Briel, U., Dennerl, K., et al. 2001, A&A, 365L, 18

Sych, R., Nakariakov, V. M., Karlicky, M., & Anfinogentov, S. 2009, A&A, 505, 791

Sych, R., & Nakariakov, V. M. 2014, A&A, 569, A72

Taroyan, Y., Erdélyi, R., Doyle, J. G., & Bradshaw, S. J. 2005, A&A, 438, 713

Trenholme, D., Ramsay, G., & Foley, C. 2004, MNRAS, 355, 1125

Tsiklauri, D., Nakariakov, V. M., Arber, T. D., & Aschwanden, M. J. 2004, A&A, 422, 351

Tsikoudi, V., & Kellett, B. J. 2000, MNRAS, 319, 1147

Turner, M. J. L., Abbey, A., Arnaud, M., et al. 2001, A&A, 365L, 27

Wang, T., Solanki, S. K., Curdt, W., et al. 2002, ApJ, 574L, 101

Wang, T. J., Solanki, S. K., Curdt, W., et al. 2003, A&A, 406, 1105

Wang, T. 2011, Space Sci. Rev., 158, 397

Watson, C. A., Dhillon, V. S., & Shahbaz, T. 2006, MNRAS, 368, 637

Wilhelm, K., Curdt, W., Marsch, E., et al. 1995, Sol. Phys., 162, 189

Wright, C. S., & Nelson, G. J. 1987, Sol. Phys., 111, 385

Wu, Z., Huang, N. E., Wallace, J. M., et al. 2011, Climate Dynamics, 37, 759

Yuan, D., Nakariakov, V. M., Chorley, N., & Foullon, C. 2011, A&A, 533, 116

Yu, S., Nakariakov, V. M., Selzer, L. A., et al. 2013, ApJ, 777, 159

Zaitsev, V. V., & Stepanov, A. V. 1982, Soviet Astronomy Letters, 8, 132

Zimovets, I. V., & Nakariakov, V. M. 2015, A&A, 577A, 4

Table 1. RHESSI Flare list for the Solar QPPs

ID	RHESSI Flare ID	Start Time of QPPs	X (")	Y (")	Period (min)	τ (min)	Significance Level
1	14010709	2014-01-07T03:35:35	-142.08	-57.37	0.903	1.118	>0.99
2	14010713	2014-01-07T03:52:58	-120.47	193.16	0.755	1.347	<0.70
3	14020696	2014-02-06T22:12:57	682.46	294.00	0.543	1.540	>0.95
4	14020697	2014-02-06T23:03:43	706.70	-182.74	1.172	2.061	>0.70
5	14020702	2014-02-07T00:36:38	700.95	-150.62	0.684	0.818	<0.70
6	14020704	2014-02-07T00:48:25	713.63	-182.77	0.724	1.389	>0.99
7	14021315	2014-02-13T05:51:37	-	-	1.765	3.788	>0.99
8	14021315	2014-02-13T05:52:26	-	-	0.878	1.573	>0.95
9	14021330	2014-02-13T06:08:05	-	-	2.074	1.904	>0.99
10	14021330	2014-02-13T06:08:16	-	-	0.346	0.570	>0.95
11	14021410	2014-02-14T02:55:21	414.43	-91.96	0.789	1.167	>0.70
12	14021410	2014-02-14T02:56:41	414.43	-91.96	0.377	0.574	>0.95
13	14021410	2014-02-14T03:04:57	414.43	-91.96	1.244	1.636	>0.70
14	14021410	2014-02-14T03:04:34	414.43	-91.96	0.831	1.331	>0.80
15	14021411	2014-02-14T03:14:60	417.46	-99.46	1.495	2.064	>0.80
16	14021417	2014-02-14T04:46:37	444.86	-72.86	1.015	2.018	>0.99
17	14021417	2014-02-14T04:47:05	444.86	-72.86	0.684	0.968	<0.70
18	14021460	2014-02-14T16:39:54	614.76	-104.82	0.437	0.806	>0.90
19	14021462	2014-02-14T17:12:16	506.00	-101.72	1.141	1.486	>0.99
20	14021462	2014-02-14T17:13:20	506.00	-101.72	0.564	0.635	>0.70
21	14021463	2014-02-14T17:23:21	512.64	-131.75	1.818	1.368	>0.99
22	14021471	2014-02-14T18:35:59	500.04	-95.24	1.471	2.533	>0.99
23	14022434	2014-02-24T12:05:31	350.59	-91.77	0.673	1.073	>0.99
24	14022434	2014-02-24T12:05:32	350.59	-91.77	0.346	1.253	>0.95
25	14022434	2014-02-24T12:16:26	350.59	-91.77	1.278	2.993	>0.99
26	14022549	2014-02-25T00:47:20	-925.93	-208.65	0.996	4.841	>0.80
27	14022813	2014-02-28T02:55:55	917.89	-170.99	0.470	0.943	>0.80
28	14022813	2014-02-28T02:57:03	917.89	-170.99	0.298	0.245	<0.70
29	14030843	2014-03-09T00:00:41	-542.15	-95.59	1.154	1.411	>0.90
30	14031016	2014-03-10T04:09:05	-689.42	-233.41	0.479	0.437	<0.70
31	14031019	2014-03-10T05:30:45	901.11	329.83	0.418	0.714	>0.95
32	14061114	2014-06-11T05:34:39	534.63	-197.99	0.247	0.340	>0.70
33	14061115	2014-06-11T05:43:42	541.50	-203.36	0.501	0.501	>0.70
34	14061115	2014-06-11T05:43:50	541.50	-203.36	0.342	0.434	>0.95
35	14061453	2014-06-14T20:17:53	883.85	-345.60	1.711	1.646	>0.90
36	14061459	2014-06-14T21:59:20	904.73	211.92	0.369	0.506	>0.80
37	14061462	2014-06-14T22:02:32	906.60	206.75	0.359	0.422	>0.95
38	14061463	2014-06-14T22:15:49	937.80	-213.53	2.116	3.957	>0.95
39	14102075	2014-10-20T20:37:48	-560.12	-326.47	0.857	1.601	>0.99
40	14102079	2014-10-20T21:07:38	-578.82	-270.98	0.710	0.680	>0.95
41	14102079	2014-10-20T21:07:48	-578.82	-270.98	0.497	0.369	>0.95
42	14102085	2014-10-20T22:48:37	-539.72	-304.12	0.772	2.103	>0.95
43	14102085	2014-10-20T22:50:08	-539.72	-304.12	0.321	0.731	>0.95
44	14102642	2014-10-26T10:06:24	515.23	-298.81	0.859	1.139	<0.70
45	14102643	2014-10-26T10:15:46	511.76	-306.18	0.668	0.927	>0.95
46	14102647	2014-10-26T11:56:41	526.39	-299.75	0.517	0.476	>0.99
47	14102648	2014-10-26T12:37:55	547.73	-299.48	2.327	3.924	>0.95
48	14102704	2014-10-27T01:52:35	670.07	-274.56	0.393	0.398	>0.80
49	14102704	2014-10-27T02:02:22	670.07	-274.56	0.902	0.949	<0.70
50	14102704	2014-10-27T02:02:28	670.07	-274.56	0.571	0.895	>0.95
51	14102709	2014-10-27T03:28:55	675.85	-277.44	0.614	1.125	>0.70
52	14102709	2014-10-27T03:41:54	675.85	-277.44	0.578	1.531	>0.95
53	14103003	2014-10-30T01:33:17	956.95	-236.79	0.478	0.623	>0.95
54	14121314	2014-12-13T05:57:08	872.87	-41.86	1.769	3.389	>0.99
55	14121314	2014-12-13T06:02:49	872.87	-41.86	0.607	0.915	>0.99
56	14121315	2014-12-13T06:35:31	351.13	-242.53	0.751	0.882	>0.70
57	14121773	2014-12-17T19:30:45	-353.72	-162.32	0.944	1.353	>0.95
58	14121773	2014-12-17T19:30:20	-353.72	-162.32	0.485	0.812	>0.70
59	14121776	2014-12-17T20:34:04	44.29	-294.75	0.394	0.708	>0.70

Table 2. XMM-Newton Target list of the stellar QPPs

ID	Target ID	Start time QPPs	Source Region[a]	Background Region[a]	Period (min)	τ (min)	Significance Level
1	0200530701	2006-05-22T01:03:28	26365,27957, 0, 600	27365,25957, 600	2.819	4.738	>0.90
2	0605581001	2009-10-07T05:20:37	27240,27401, 300	27240,27401, 300, 500	55.677	111.966	>0.80
3	0602290101	2009-05-06T23:11:50	26415,27947, 0, 600	24415,29947, 600	57.774	71.784	<0.70
4	0111460101	2000-10-09T14:20:43	24987,24162, 100, 800	25687,27662, 800	7.041	12.963	<0.70
5	0111520101	2001-09-11T06:38:13	23904,25690, 75, 600	25204,29190, 600	5.544	11.298	>0.70
6	0551020101	2008-09-05T17:32:38	27083,27641, 0, 500	26083,25641, 500	15.071	21.933	>0.80
7	0672390201	2011-05-01T06:35:43	24304,24486, 0, 300	25304,25486, 300	10.276	11.415	<0.70
8	0672390201	2011-05-01T06:35:43	24304,24486, 0, 300	25304,25486, 300	18.383	36.919	>0.80
9	0111420101	2000-10-14T06:06:52	27525,27113, 120, 800	28525,23613, 800	8.560	11.815	>0.70
10	0111420101	2000-10-13T17:33:52	27525,27113, 120, 800	28525,23613, 800	8.543	27.472	<0.70
11	0111420101	2000-10-13T17:33:52	27525,27113, 120, 800	28525,23613, 800	15.516	21.832	>0.70
12	0111420101	2000-10-13T17:21:52	27525,27113, 120, 800	28525,23613, 800	5.237	9.405	>0.80
13	0112530101	2002-09-15T22:28:04	22517,19333, 0, 400	22517,19333, 500, 700	51.783	70.107	>0.95
14	0041741101	2004-05-01T16:21:50	23959,24366, 300	23261,23661, 300	24.542	35.333	>0.95
15	0300170101	2006-02-19T10:05:38	27398,27296, 0, 500	27898,25796, 500	3.011	4.352	>0.80
16	0300170101	2006-02-19T10:05:38	27398,27296, 0, 500	27898,25796, 500	5.171	7.674	>0.90
17	0300170101	2006-02-19T10:05:38	27398,27296, 0, 500	27898,25796, 500	7.552	17.107	>0.90
18	0300170101	2006-02-19T10:05:38	27398,27296, 0, 500	27898,25796, 500	13.935	16.468	>0.99
19	0143630101	2004-11-03T01:27:28	26575,27303, 0, 350	27575,26303, 300	10.904	16.910	>0.99
20	0143630101	2004-11-03T01:27:28	26575,27303, 0, 350	27575,26303, 300	20.213	41.386	<0.70
21	0049350101	2001-08-12T18:08:42	26761,27721, 200, 800	26661,24221, 600	11.127	23.597	>0.95
22	0049350101	2001-08-12T18:26:42	26761,27721, 200, 800	26661,24221, 600	18.161	33.608	>0.99
23	0056030101	2001-01-19T16:58:52	25335,23878, 0, 500	25335,23878,1000,1200	11.854	13.203	<0.70
24	0056030101	2001-01-19T18:48:52	25335,23878, 0, 500	25335,23878,1000,1200	22.120	29.424	<0.70
25	0056030101	2001-01-19T17:00:32	25335,23878, 0, 500	25335,23878,1000,1200	20.339	30.948	>0.90
26	0551120201	2009-03-12T10:32:29	26293,23785, 0, 700	24293,26285, 700	19.745	27.211	>0.95
27	0551120201	2009-03-12T07:22:29	26293,23785, 0, 700	24293,26285, 700	6.024	5.811	>0.80
28	0203260101	2004-08-01T12:14:47	24232,24428, 50, 400	23232,28428, 400	34.487	76.098	>0.90
29	0101440201	2002-08-13T11:56:41	24126,26954, 0, 700	26021,27451, 700	30.720	29.170	>0.95
30	0551120401	2009-03-14T07:10:07	26410,23921, 0,1000	23910,26421,1000	3.707	6.424	>0.90
31	0551120401	2009-03-14T07:10:07	26410,23921, 0,1000	23910,26421,1000	12.264	16.503	>0.95
32	0551120401	2009-03-14T07:10:07	26410,23921, 0,1000	23910,26421,1000	21.025	19.263	>0.95
33	0111180201	2001-11-08T04:08:37	27733,27228, 150, 800	29251,29691, 800	2.129	3.490	>0.90
34	0111180201	2001-11-08T03:57:37	27733,27228, 150, 800	29251,29691, 800	8.821	35.887	>0.99
35	0112880801	2000-09-30T01:18:07	25381,23911, 0, 600	26881,20911, 600	19.356	37.853	<0.70
36	0112880801	2000-09-30T01:19:47	25381,23911, 0, 600	26881,20911, 600	36.740	50.015	>0.95
37	0200530301	2005-12-11T09:21:41	26008,23596, 0, 600	25008,26596, 600	9.062	9.670	>0.95
38	0200530501	2006-05-20T02:49:48	26375,27948, 0, 600	27375,24948, 600	2.384	4.576	>0.99
39	0200530501	2006-05-20T00:47:38	26375,27948, 0, 600	27375,24948, 600	1.690	3.434	>0.90
40	0200530501	2006-05-20T00:47:08	26375,27948, 0, 600	27375,24948, 600	2.611	4.898	>0.95
41	0123710101	2000-04-25T04:50:38	26590,27922, 75, 800	28790,25122, 800	8.025	13.222	>0.80
42	0148440101	2002-12-17T01:27:20	31082,12632, 0, 200	31082,13632, 150	19.920	16.000	<0.70
43	0601950101	2010-03-20T00:46:02	24545,24459, 100, 700	23045,27959, 700	7.899	10.854	>0.95
44	0551120301	2009-03-10T03:46:59	26171,23861, 0, 700	24671,26361, 700	8.358	15.876	>0.99
45	0041750101	2002-06-16T00:56:54	21977,19169, 0, 200	20869,18565, 200	64.965	114.735	>0.80
46	0041750101	2002-06-15T21:13:34	21977,19169, 0, 200	20869,18565, 200	69.537	74.508	>0.70
47	0111510101	2000-10-16T06:34:41	27480,27081, 75, 800	27980,24081, 800	8.641	15.956	>0.80
48	0111510101	2000-10-16T06:34:41	27480,27081, 75, 800	27980,24081, 800	13.402	18.012	<0.70
49	0200530801	2006-05-24T00:34:58	26322,27936, 0, 400	26322,26436, 400	1.965	2.539	>0.95
50	0111410101	2002-02-09T22:09:31	27483,27159, 0, 800	27483,27159, 800,1100	28.572	72.771	>0.90
51	0111410101	2002-02-09T22:09:31	27483,27159, 0, 800	27483,27159, 800,1100	52.055	94.302	>0.70
52	0551022901	2008-09-06T08:47:09	27536,27082, 0, 250	26536,27082, 250	2.452	3.625	<0.70

[a]Annulus (X, Y, R_1, R_2) or in circle (X, Y, R)

Table 3. Statistics of the Period and Damping time

Parameter	Solar QPPs	Stellar QPPs	K-S Test
$P(min)$	0.90 ± 0.56	16.21 ± 15.86	
$\tau(min)$	1.53 ± 1.10	27.21 ± 28.73	
τ/P	1.74 ± 0.77	1.69 ± 0.56	p-value= 0.93[a]

[a]The small p-value (e.g., 0.01) indicates that the cumulative distributions are significantly different from each other.

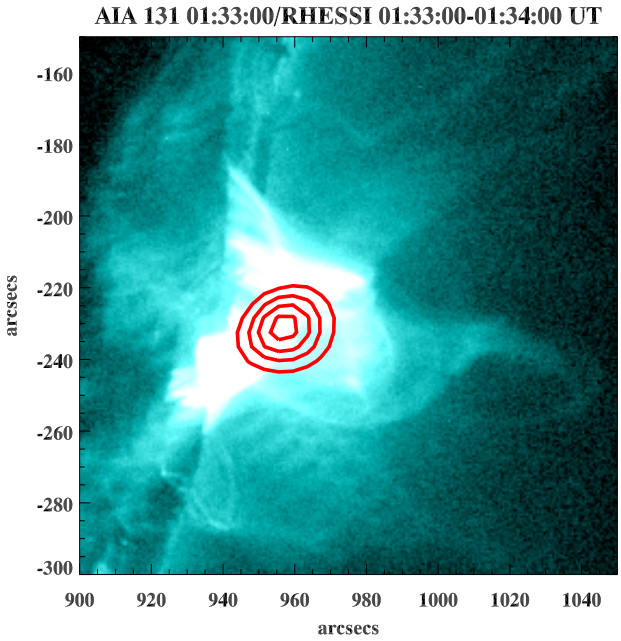

Fig. 1.— Example of a solar flare observed at 30 Oct 2014 01:33:00 UT. The red contours correspond to the **30%, 50%, 70%, and 90%** count levels relative to the maximum X-ray counts measured by RHESSI in the 3–12 keV channel. The soft X-ray emission contours are superimposed on the EUV image obtained with SDO/AIA at 131Å.

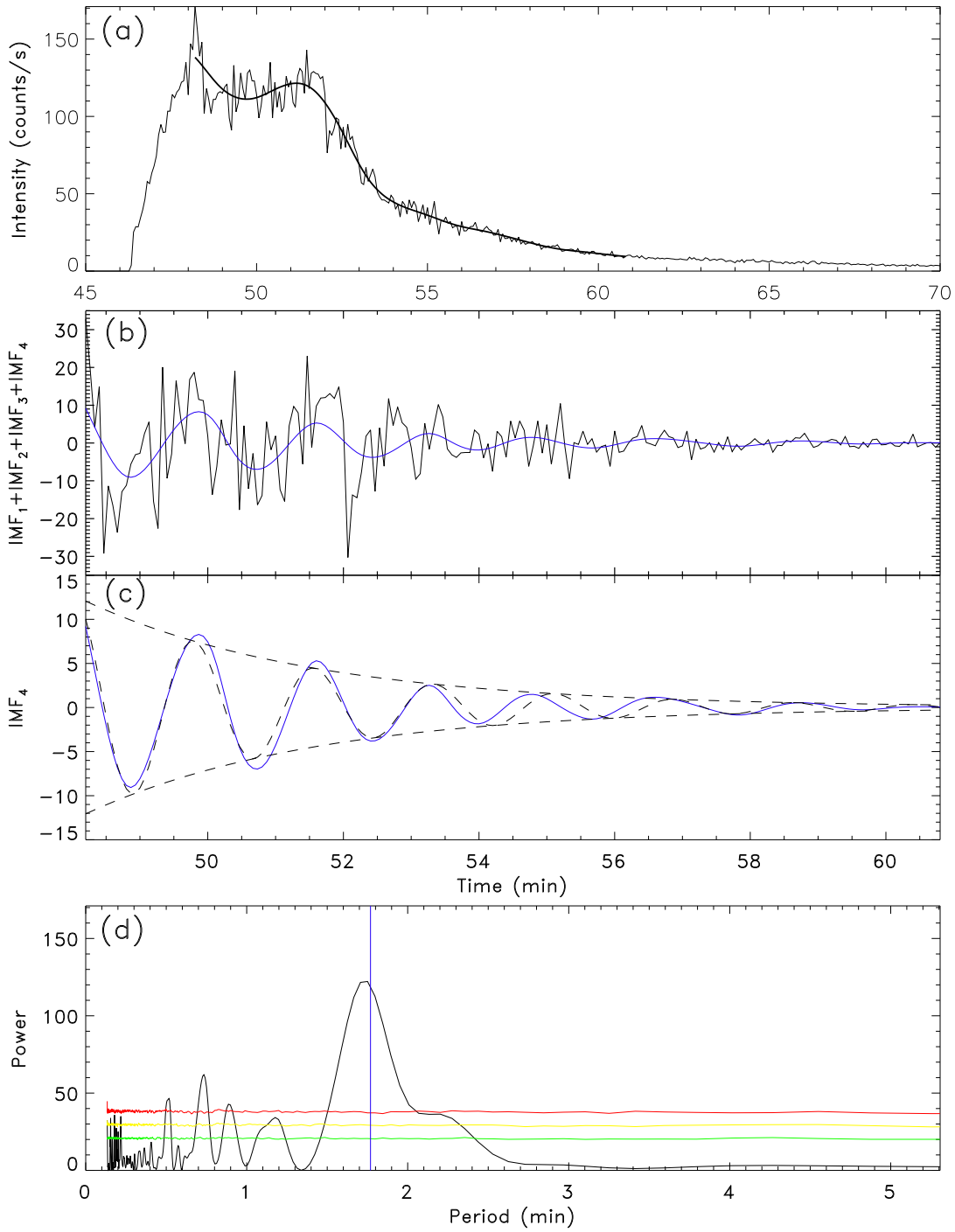

Fig. 2.— Example of an X-ray light curve of a solar flare observed with RHESSI at the 3-24 keV energies, panel (a). The smoothed solid line is the trend obtained by applying the Empirical Mode Decomposition technique. The residual signal obtained by de-trending, consisting of several intrinsic mode functions (IMF) is shown in panel (b). The blue curve shows the damped oscillatory IMF. Panel (c) shows the best-fitting of the IMF by a decaying harmonic oscillation (the black dashed curve). Panel (d) shows the power spectrum of the residual signal given in panel (b). The blue-vertical line is the period obtained from fitting by the least-square technique. The red, yellow, and green curves are 99%, 95%, and 90% confidence intervals.

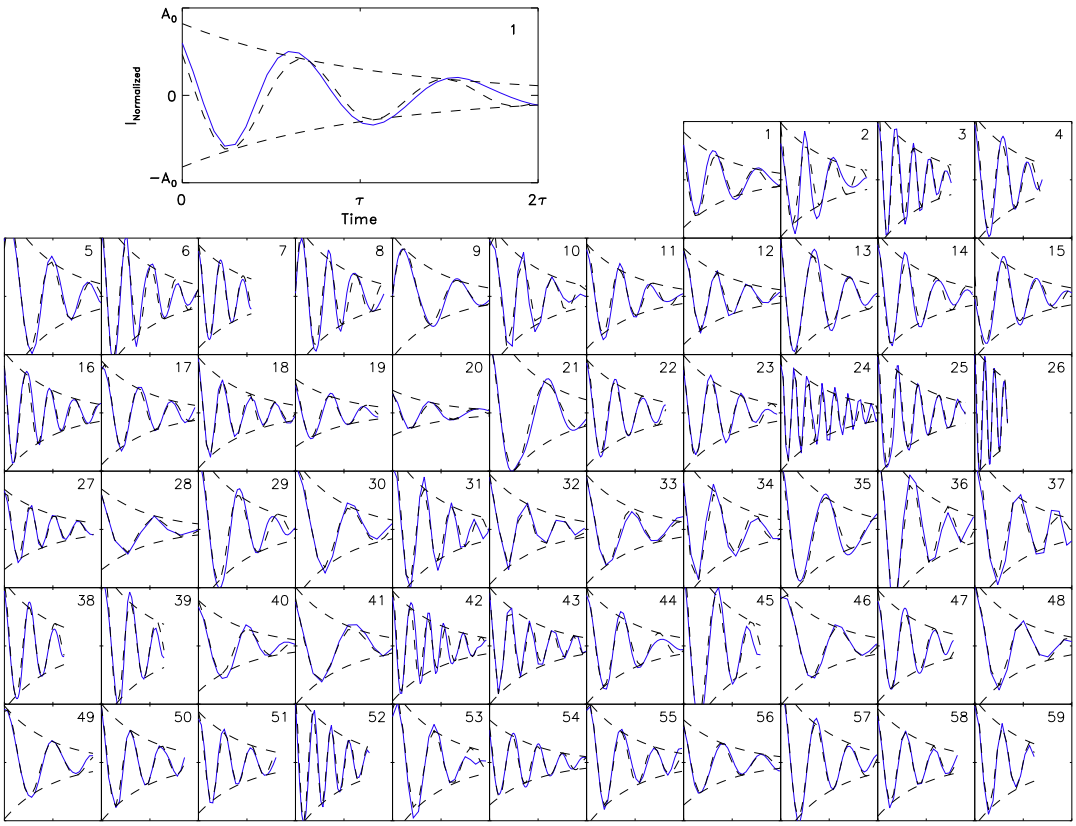

Fig. 3.— The 59 candidates for the solar flaring QPPs (blue) with their damped harmonic fit (dashed). The scales of the horizontal and vertical axes are normalized to the maximum amplitudes of the exponential function and damping times, respectively, as it is shown in the zoomed plot of the first sample.

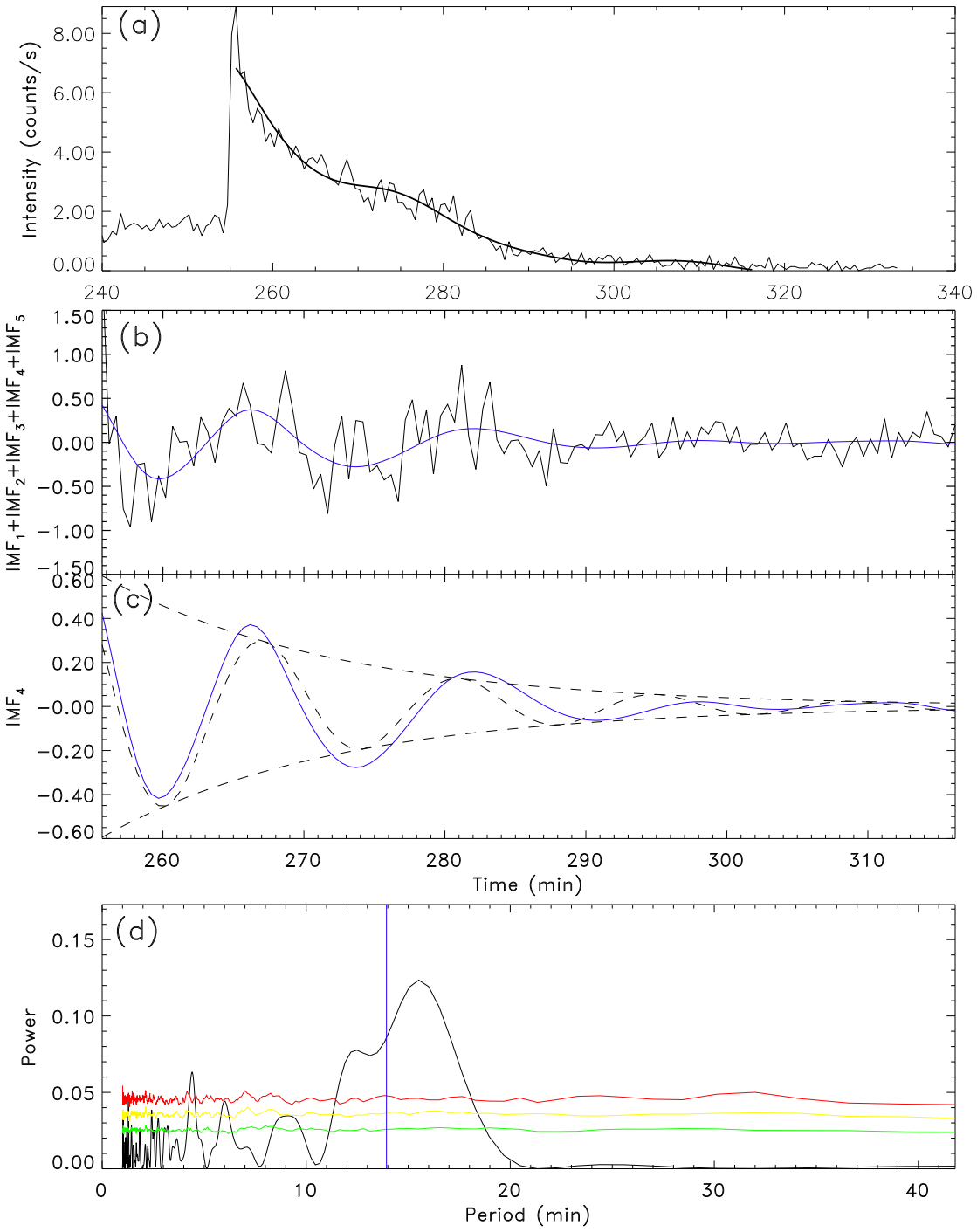

Fig. 4.— Example of a XMM-Newton light curve with the smooth trend (the solid curve) obtained by applying the Empirical Mode Decomposition technique, panel (a). The residual signal obtained by de-trending, consisting of several intrinsic mode functions (IMF) is shown in panel (b). The blue curve shows the damped oscillatory IMF. Panel (c) shows the best-fitting of the IMF by a decaying harmonic oscillation (the black dashed curve). Panel (d) shows the power spectrum of the residual signal given in panel (b). The blue-vertical line is the period obtained by best fitting. The red, yellow, and green curves are 99%, 95%, and 90% confidence intervals.

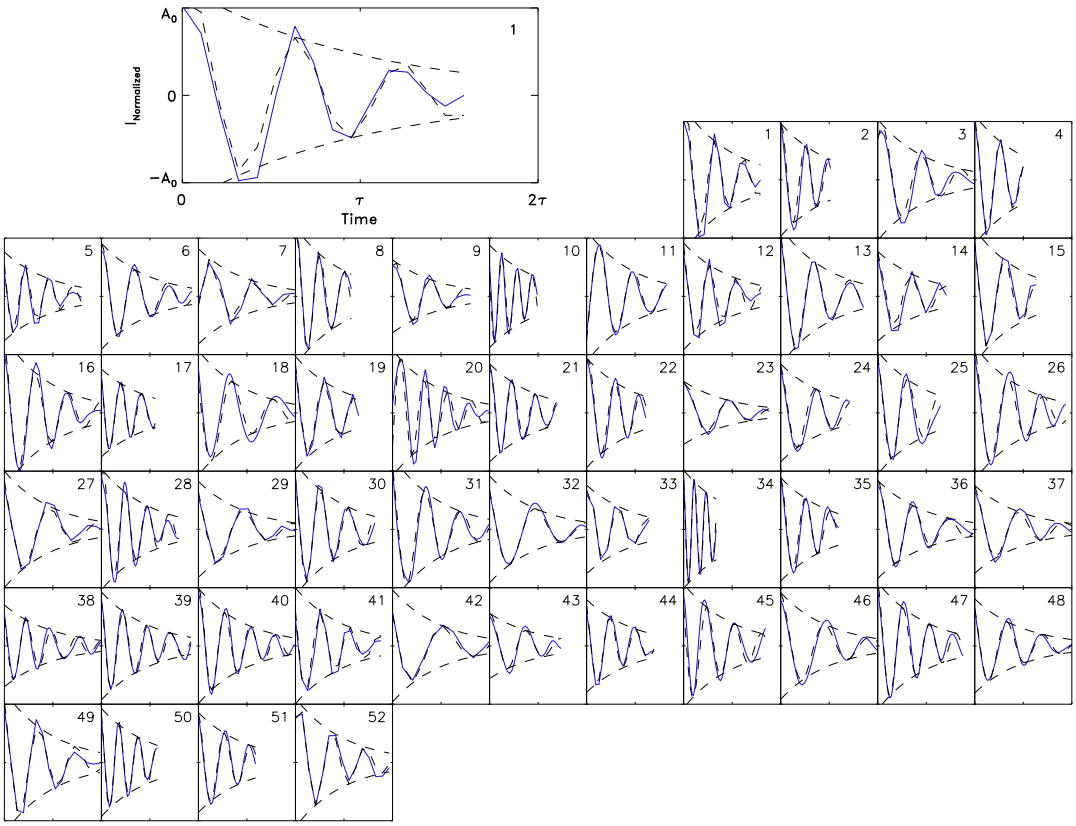

Fig. 5.— QPPs in stellar flares (blue) and the best-fitting damped harmonic functions (dashed). For visualization, the scales of the horizontal and vertical axes are normalized to the maximum amplitudes of the exponential function and damping times, as shown in the zoomed plot for the first sample.

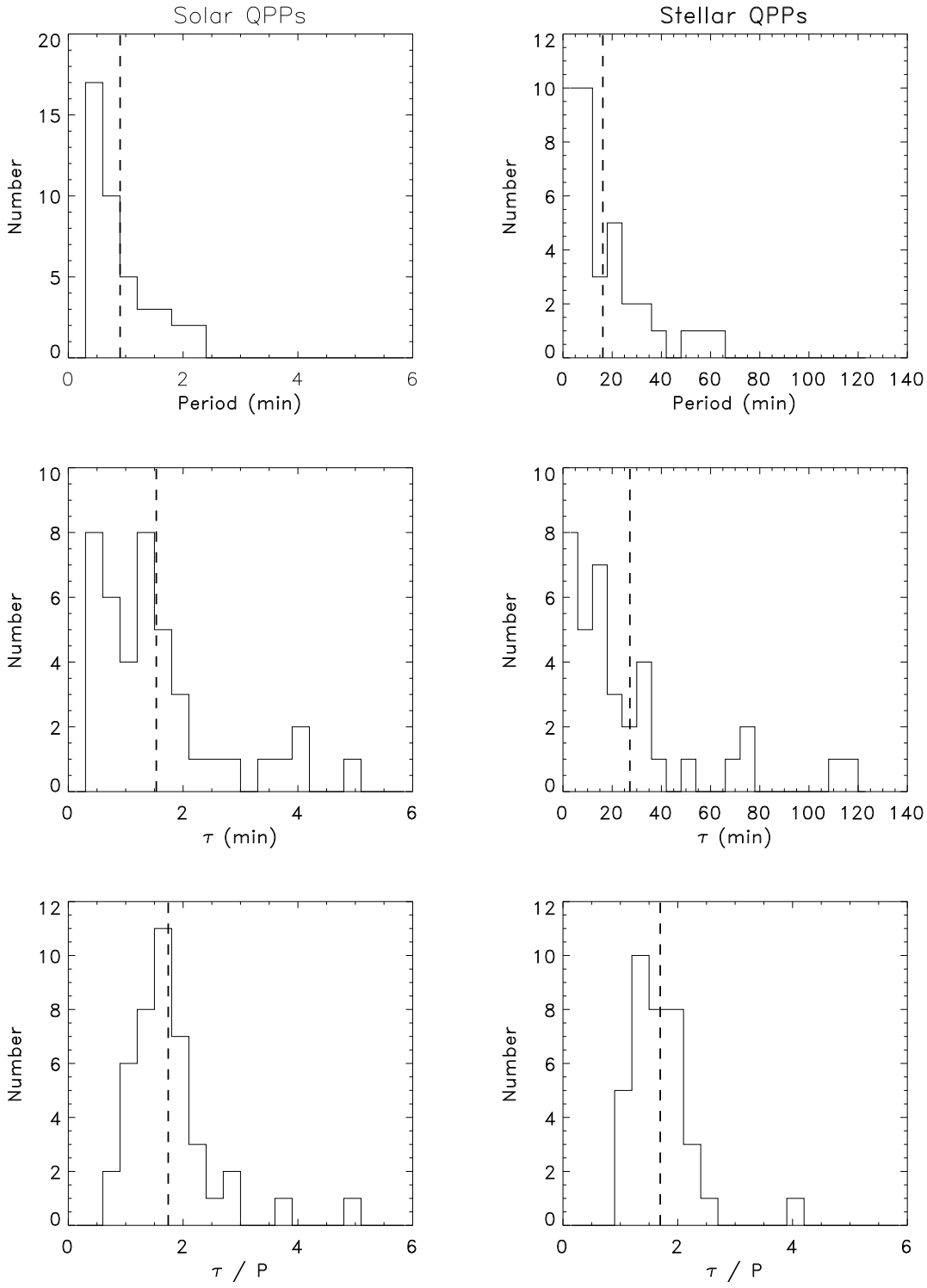

Fig. 6.— Distributions of the periods, damping times, and their ratios for the solar (left) and stellar (right) QPPs. Vertical dashed lines in each panel indicate their mean values.

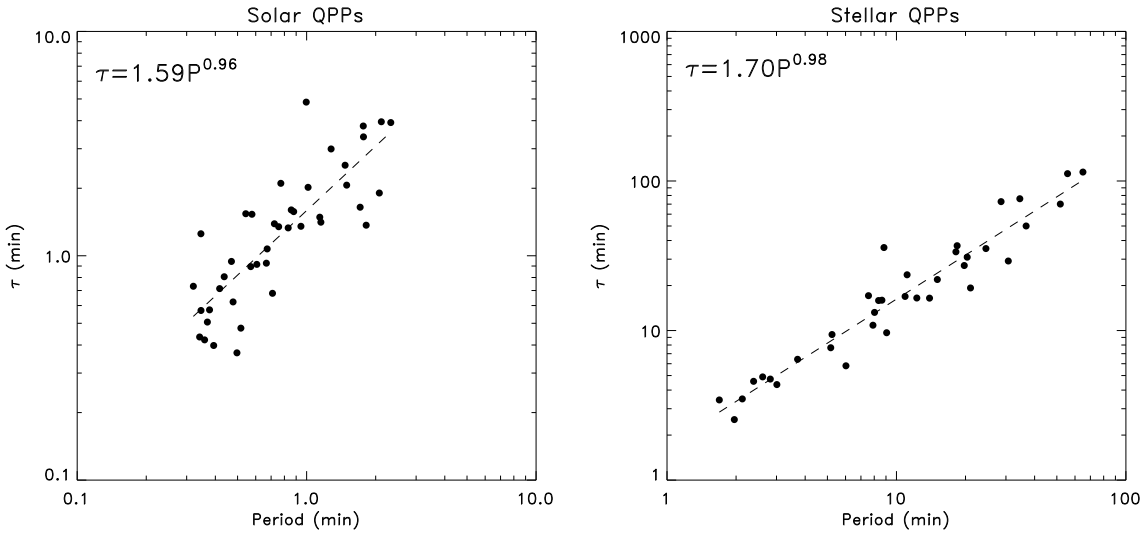

Fig. 7.— Damping times as a function of the period for solar (left) and stellar QPPs (right). The dashed lines show the least-square power-law fits.

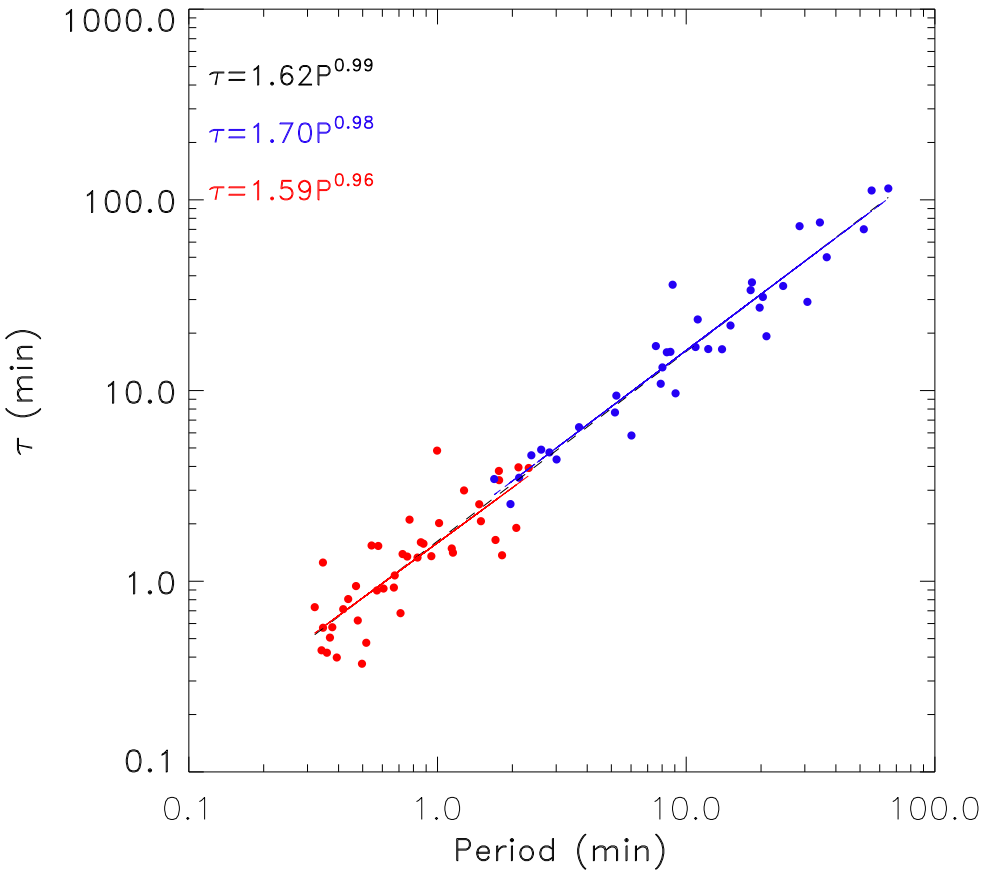

Fig. 8.— Damping times as a function of the period for the solar (red) and stellar QPPs (blue). The blue and red straight lines show the best-fitting power-law dependency. The black dashed line is the least-square-fit with the form of $\tau = 1.62 \times P^{0.99}$, where P and τ are periods and damping times, respectively, of the combined, solar and stellar, sets of QPPs.